Solitary waves perturbed by a broad sill. Part 1. Propagation across the sill

Harrison T.-S. Ko¹ and Harry Yeh^{1,†}

¹Department of Civil and Construction Engineering, Oregon State University, Corvallis, OR 97331, USA

(Received 6 March 2019; revised 23 June 2019; accepted 22 August 2019)

Stability of a solitary wave disturbed by a submerged flat sill is investigated experimentally. For sills narrow compared with the solitary wave, the transmitted waves are found to be unaffected in waveform and amplitude. A wider sill disturbs the solitary wave resulting in the formation of a dispersive wavetrain following the transmitted wave. In some cases, the wave amplitude recovers, despite being perturbed, to the state of an unobstructed solitary-wave state at a certain distance beyond the sill. Wider sills cause wave breaking that occurs over the sill or, in some cases, after the wave passes through the sill. Details of waveform transformation leading toward the breaking and subsequent energy dissipation are discussed.

Key words: wave breaking, solitary waves, surface gravity waves

1. Introduction

Solitary waves have been used in the literature to study the characteristics and behaviour of weakly nonlinear localized long waves. Extensive attention has been given to the run-up of solitary waves on sloping beaches (e.g. Goring 1978; Pedersen & Gjevik 1983; Kobayashi, Otta & Roy 1987; Synolakis 1987; Kobayashi, DeSilva & Watson 1989; Lin, Chang & Liu 1999; Carrier, Wu & Yeh 2003; Li & Raichlen 2003; Hsiao et al. 2008; Knowles & Yeh 2018), fission and breaking from wave propagation over submerged steps (e.g. Losada, Vidal & Medina 1989; Yasuda, Mutsuda & Mizutani 1997; Liu & Cheng 2001) and vortex evolution and advection around a submerged obstacle (e.g. Chang, Hsu & Liu 2001; Huang & Dong 2001; Lin et al. 2006; Lin & Huang 2010). In addition, performance of a submerged breakwater has been investigated extensively using solitary waves (e.g. Mei & Black 1969; Massel 1983; Seabra-Santos, Renouard & Temperville 1987; Grue 1992; Rey, Belzons & Guazzelli 1992; Ting & Kim 1994; Zhuang & Lee 1997; Tang & Chang 1998; Huang & Dong 1999; Chang et al. 2001; Chang, Hsu & Liu 2005).

Solitary-wave interaction with a submerged sill has received some attention in the literature. Here we use the term 'sill' to represent a straight and uniform underwater ridge that divides a water body of uniform depth. The characterization of the wave-sill interaction has been focused on reflection and transmission coefficients (Lin 2004). Studies involving monochromatic waves have identified that the height of the sill is important for determining these coefficients (e.g. Losada, Silva & Losada 1996;

Christou, Swan & Gudmestad 2008; Young & Testik 2011). Analytical studies on solitary wave interaction with a submerged sill has been limited (Lin 2004; Lin & Liu 2005). Instead, most studies that characterize wave-sill interaction have been primarily numerical and experimental.

Seabra-Santos et al. (1987) examined the motion of solitary waves over a submerged triangular-shaped sill. Their study predicts reflection and the formation of a perturbed transmitted wave with a trailing, small-amplitude dispersive wavetrain. Cooker et al. (1990) extended this work by studying solitary-wave interaction with a submerged semicircular sill, using an extension of the numerical model by Dold & Peregrine (1986). Results from Cooker et al. (1990) found a variety of different interactions that depend on the wave height and semicircular-sill size. Four types of interactions were described: small dispersive wavetrain development behind the transmitted wave, crest-crest exchange, forwards breaker and backwards breaker. These results were confirmed by a limited number of experiments, although the backwards breaker was not observed in the laboratory. Grilli, Losada & Martin (1994) expanded this work to trapezoidal-shaped obstacles (a model of a submerged breakwater) and characterized wave behaviour as a function of the obstacle and incident wave height. Their laboratory observations found that the waves may break forwards or backwards downstream of the obstacle.

In the present study, we expand the experimental work of Seabra-Santos et al. (1987), Cooker et al. (1990) and Grilli et al. (1994) to study the effect of sill's breadth on the transmitted solitary waves. Here we use a rectangular-shaped flat plate for the sill. We focus on the transformation of the solitary wave at a significant distance after interaction with the sill, as well as the characterization of wave behaviour over the sill. It is noted that, in a companion paper (Part 2, Yeh et al. 2019), we study the effect of a submerged sill placed along the direction of wave propagation; in other words, the uniform disturbance is applied to a finite breadth continually along the propagation.

2. Laboratory experiments

2.1. Experimental set-up

Experiments are performed in a wave tank with a submerged rectangular-shaped sill spanning the width of the tank: see figure 1. The wave tank, 7.3 m long, 2.5 m wide and 0.30 m deep, is elevated 1.2 m above the laboratory floor. The bottom and side walls of the tank are made of 12.7 mm thick glass plates. This design facilitates the use of optical techniques to measure wave fields. As discussed later, the glass bottom eliminates laser-sheet reflection; such reflection can cause substantial noise in wave-profile measurements from the laser-induced fluorescence (LIF) technique. The tank bed was levelled to form the horizontal plane with a tolerance of ± 0.8 mm. This degree of precision is important for the study of nonlinear 'long' waves. The wave tank is relatively wide in comparison with the water depth – the quiescent water depth is set at $h_0 = 5.0$ cm in this study – so that any disturbance that may be created along the side walls should be negligible.

The wave basin is equipped with a wavemaker along the 2.5 m long head wall, capable of generating arbitrarily shaped waves. The wave paddles are pushed by linear motors, which are inherently more accurate for producing linear positioning than traditional rotary motors. The maximum horizontal stroke for the wave paddles is 55 cm – adequate for the generation of long waves in the water depth of $h_0 = 5.0$ cm. (In the present experiments, the maximum stroke used was 9.0 cm.) The generated

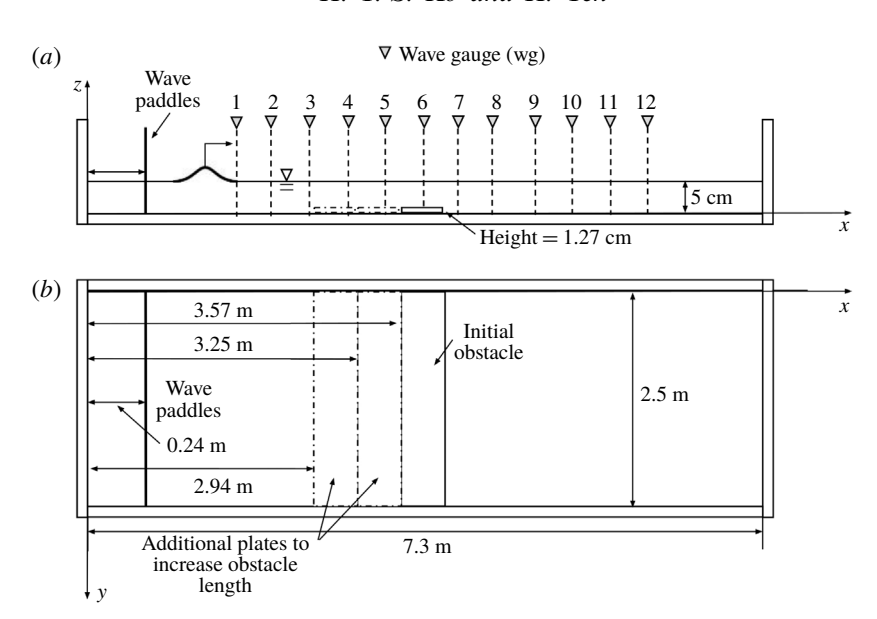


FIGURE 1. Schematic drawings of the wave tank: (a) elevation view showing the position of wave gauge measurements; (b) plan view showing the position of three different submerged sill breadths. To fit the glass plate, the tank breadth is narrowed by placing a vertical rigid waveguide (one of the side walls shown in (b) is the waveguide). The coordinate system defined in the figure is used to describe positioning within the wave tank.

waves are repeatable: Li, Yeh & Kodama (2011), who performed their experiments using the same apparatus, reported that the maximum error for a solitary wave was less than 0.1% of the depth when the wave amplitude was 1.73 cm in water depth $h_0 = 6.0$ cm.

Figure 1 shows a schematic sketch of the experimental set-up with the submerged sill placed in the transverse orientation. Glass plates are used to create the sill. Each glass plate has dimensions of 0.3175 m in width and 0.0127 m in height, and spans 2.5 m from side wall to side wall. The plate is placed directly on the tank bottom oriented such that the 2.5 m dimension is perpendicular to the direction of wave propagation. Three glass plates are used to create sills of different breadths (0.3175 m, 0.6350 m, 0.9525 m). The initial glass plate is placed with its upstream edge at 3.57 m from the wave tank head wall. The subsequent glass plates, for changing the sill breadth, are placed on the upstream side of the initial sill to maximize the post-sill propagation distance in the wave tank. It is noted we add a rigid vertical waveguide along the tank to match the sill (comprised of glass plates) dimensions with the width of the tank.

2.2. Wave generation and measurements

To generate clean solitary waves, we use the higher-order solution by Grimshaw (1971), which is presented explicitly by Tanaka (1993). In non-dimensionalized form with the use of the ambient water depth h_0 for the length scale and $t_0 = \sqrt{h_0/g}$ for the time scale (g is the gravitational acceleration), the water-surface elevation η of the higher-order solitary wave can be expressed as

$$\eta = as^2 - \frac{3}{4}a^2(s^2 - s^4) + a^3\left(\frac{5}{8}s^2 - \frac{151}{80}s^4 + \frac{101}{80}s^6\right),\tag{2.1}$$

where a is the normalized wave amplitude, $s \equiv \operatorname{sech}(\alpha(x - Ft)), F = 1 + \frac{1}{2}a$ $\frac{3}{20}a^2 + \frac{3}{56}a^3$, $\alpha = \sqrt{\frac{3}{4}}a(1 - \frac{5}{8}a + \frac{71}{128}a^2)$, t is the normalized time and x points in the propagation direction. With η obtained from (2.1), we first compute the depth-averaged fluid velocity by $\bar{u} = F\eta/(1+\eta)$, then find the wave-paddle displacement, x, by integrating $dx/dt = \bar{u}(x, t)$.

Water-surface measurements are made using four ultrasonic wave gauges (General Acoustics, Model HF54 Controller and USS 02-HF Sensors). The wave gauge system uses non-intrusive devices that avoid the uncertainty of meniscus effects inherent to standard intrusive wave gauges (e.g. capacitance and resistance types gauges). This wave gauge system operates at a sampling rate of 50 Hz and has a resolution of 0.18 mm. As shown in figure 1, wave gauge measurements are taken at twelve locations for each experimental run. Since only four wave gauges are available, experiments for each condition are repeated three times. The wave gauges are attached to movable carriages and traversed from location to location in between repeated runs. It is emphasized that this laboratory apparatus together with the wavemaker system is capable of generating a precisely repeatable wave.

The LIF technique is implemented to capture the detailed wave breaking processes. The LIF technique has been used to optically record the temporal variation of the air—water interface of long waves (Yeh & Ghazali 1987; Ramsden & Raichlen 1990; Duncan et al. 1994, 1999; Gardarsson & Yeh 2007; Diorio, Liu & Duncan 2009). In the present study, the LIF method comprises of a 5 W diode-pumped solid-state laser, cylindrical lens and two front-face mirrors. The laser beam is converted to the laser sheet by the cylindrical lens, and then the laser sheet is directed to the desirable direction and location with the use of two front-face mirrors. A thin laser sheet illuminates the dyed water from above, then the dissolved fluorescein in the illuminated plane is activated and becomes fluorescent. The water surface along the illuminated line is captured with a video camera (1696 \times 1710 pixels). The captured images are rectified and processed so that the resulting images are analysed quantitatively. This technique accurately obtains temporal and spatial variations of the water surface in a non-intrusive manner at a frequency of 100 Hz.

One of the difficulties associated with the LIF technique arises from its application to images associated with a very large (or small) aspect ratio: capturing long waves with the LIF technique is not straightforward because of its inherently small vertical-to-horizontal length scale ratio. This results in insufficient resolution in the vertical direction. To circumvent this difficulty, we repeat LIF water-surface profiles on approximately 27 cm segments, and make a montage of the multiple-segment profiles to cover a sufficient span of the wave evolution. This procedure is only possible with a laboratory apparatus that is capable of precise replication. The same procedure was used previously in this laboratory for the measurements of Mach reflection by Li et al. (2011) and solitary-wave collisions by Chen & Yeh (2014).

2.3. Experimental conditions

The water depth for the experiments is maintained at $h_0 = 5.0$ cm. From hereinafter, the parameters with the subscript '0' represent the dimensional quantities. At this water depth, six different solitary-wave conditions are generated with amplitudes of $a_i (= a_0/h_0) = 0.1, 0.2, 0.3, 0.4, 0.5$ and 0.6. For three sill breadths, there are a total of 18 conditions which are shown in table 1. In the table, $D = (D_0/h_0)$ is the breadth of the submerged sill, and D/l is the relative length scale of the submerged disturbance to the length of solitary wave, in which the effective wavelength, $l = (l_0/h_0)$, is taken

	D = 6.35		D = 12.70		D = 19.05	
a_i	D/l	Response	D/l	Response	D/l	Response
0.1	0.95	U (1.0)	1.89	U (8.2)	2.84	S(-2.0)
0.2	1.34	S(-0.5)	2.68	S (1.9)	4.02	J (2.8)
0.3	1.64	S(-0.3)	3.28	J (5.7)	4.92	J (7.2)
0.4	1.89	J (2.9)	3.79	J (9.5)	5.68	J (11.6)
0.5	2.12	J (5.4)	4.24	B (11.5)	6.35	B (23.1)
0.6	2.32	B (7.1)	4.64	B (22.7)	6.96	B (35.1)

TABLE 1. Experimental cases: a_i is the amplitude of the solitary wave; l is the effective length of the solitary wave based on (2.2); D refers to the breadth of the sill. Wave response is expressed as: U for 'unperturbed', S for 'small perturbation', J for 'large perturbation' and B for 'wave breaking. The numbers in parenthesis are the per cent (%) loss in the total mechanical energy in comparison with the corresponding unobstructed solitary wave. Any negative value in energy loss is non-physical and must be the result of insufficient wave gauge resolution for the cases of small-amplitude waves. Details of the different responses and energy losses will be discussed in § 3 and also presented graphically in figure 10.

as the distance for which 95 % of the volume is contained (Dean & Dalrymple 1991) and is given by

$$l = \frac{2.12}{\sqrt{a}}.\tag{2.2}$$

Because the quiescent water depth h_0 is fixed at 5.0 cm, the height of the sill is also fixed: $b = (b_0/h_0) = 0.254$ for all the cases studied here. In addition to the cases represented in table 1, unobstructed cases were observed by measuring the solitarywave amplitude decay rate in the wave tank for each a_i used in these experiments.

3. Results

As mentioned, prior to examining solitary waves disturbed by the submerged sills, we first measure the 'unobstructed' wave amplitude decay in the wave tank (with no sill in the tank). The amplitude attenuation rate of solitary waves can be estimated theoretically based on energy dissipation in the thin laminar boundary layer on the bed (Keulegan 1948), and it is written in the non-dimensionalized form

$$a^{-1/4} - a_i^{-1/4} = Kx, (3.1)$$

where the coefficient of damping K is

$$K = \frac{1}{12} \sqrt{\frac{\nu}{g^{1/2} h_0^{3/2}}},\tag{3.2}$$

for a very wide channel, and ν is the kinematic viscosity of water. Note that Keulegan's original (1948) analysis includes the effect of tank side walls. In the present experiments, the tank is very wide: the ratio of the depth to the tank breadth is $h_0/B = 1/50$. Hence the energy dissipation caused by the side walls is neglected.

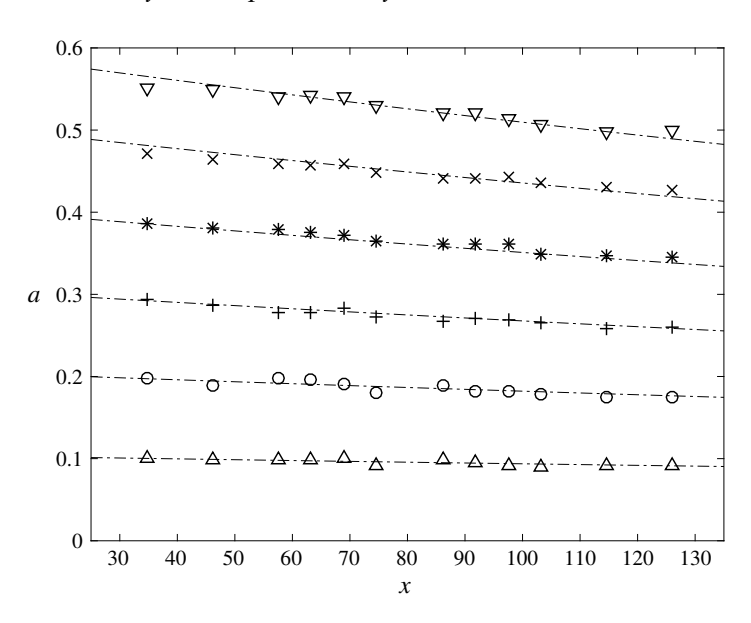


FIGURE 2. Attenuation of unobstructed solitary-wave amplitudes: \triangle , $a_i = 0.1$; \bigcirc , $a_i = 0.2$; $+, a_i = 0.3; *, a_i = 0.4; \times, a_i = 0.5; \nabla, a_i = 0.6; -\cdot-\cdot$, prediction by (3.1).

In (3.1) and (3.2), a is the wave amplitude after travelling distance x, and a_i is the initial wave amplitude.

Figure 2 exhibits the comparison of the measured amplitude attenuation with the prediction made by (3.1). The agreement is excellent even for the highly nonlinear cases. The excellent agreement must be due partly to the use of very wide wave tank; hence complex energy dissipation in the side wall boundary layer, and perhaps more important, the effect of energy exchange through the confluence of the side wall and water surface is negligible in comparison with the energy dissipation in the bed boundary layer. According to Miles (1967) and Mei & Liu (1973), the small region of the water surface near the side wall plays an important role in feeding wave energy into the side wall boundary layer, which leads to energy dissipation.

As presented in table 1, solitary-wave evolution through the disturbance of the submerged sill is categorized by four classes: (i) unperturbed, (ii) small perturbation, (iii) large perturbation and (iv) wave breaking. Figure 3 exhibits the transformation of wave profiles for those four classes. We present the representative cases for each class, namely (a) $(a_i = 0.1, D/l = 0.947)$ for unperturbed; (b) $(a_i = 0.3, D/l = 1.64)$ for small perturbation; (c) $(a_i = 0.4, D/l = 5.68)$ for large perturbation; (d) $(a_i = 0.5, 0.5)$ D/l = 6.35) for wave breaking. In addition, in figure 4, we present the evolution of the amplitudes for those four cases.

3.1. Unperturbed

The water-surface data for the case of $a_i = 0.1$ with D/l = 0.947 in figure 3(a) show that the submerged sill had a negligible effect on the solitary wave passing over it. The transmitted wave shows no sign of the formation of a trailing dispersive wavetrain and the wave profile matches the theoretical solitary-wave profile at each location. Figure 4(a) indicates that the amplitude attenuation is essentially the same as the condition without the sill that is predicted by (3.1); some observed deviations are

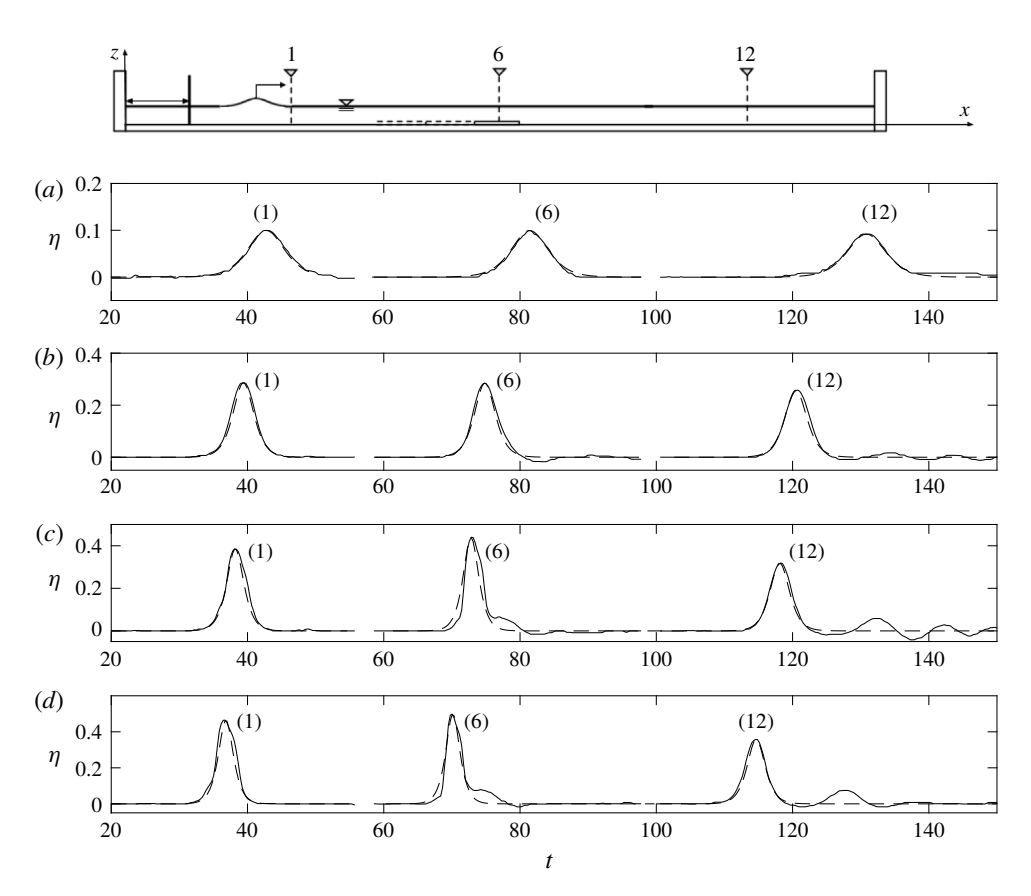


FIGURE 3. Time variation of the water-surface profile at x = 34.8 (at the gauge location (1) as indicated in figure 1: close to the wave paddle), x = 74.7 (at the gauge location (6) above downstream end of the sill) and x = 126.0 (at the gauge location (12) near the end of the tank): (a) for the wave $a_i = 0.1$ passing over a submerged sill of breadth D/l = 0.947; (b) $a_i = 0.3$, D/l = 1.64; (c) $a_i = 0.4$, D/l = 5.68; (d) $a_i = 0.5$, D/l = 6.35. The solid line, —, represents the measured data. The dashed line, —, represents the theoretical third-order solitary wave solution from (2.1).

likely due to the resolution of the wave gauges. Although not shown for brevity, the reflected wave from the upstream edge of the sill was found to be extremely small, if it existed at all, and could not be distinguished from the measurement noise of the wave gauge at x = 34.8 (location (1) shown in figure 1). The lack of a reflected wave observed in this case is consistent with experimental results from the study performed by Seabra-Santos et al. (1987). They found that reflected waves were negligible for sills smaller than half the depth. Despite the difference in geometry (triangular-shaped sills used by Seabra-Santos et al. (1987) and rectangular sills used in the present study) results for the small D/l = 0.947 case are consistent with their observations.

As stated, the 'unperturbed' label describes an unnoticeable solitary wave response to the sill. The stability of the solitary wave persists, and the amplitude remains practically at the same level as the state of free propagation without a sill. It is noted that similar behaviour, that is categorized as 'unperturbed', is observed for the case of $(a_i = 0.1, D/l = 1.89)$ as presented in table 1. This interaction occurs when the

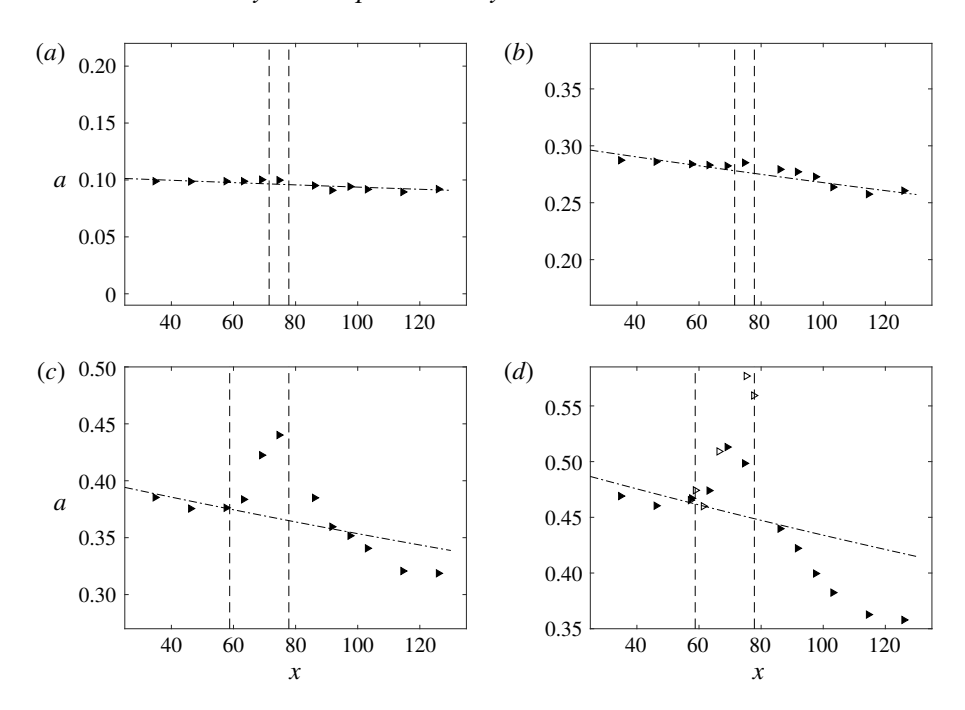


FIGURE 4. Wave amplitude evolution: (a) for a wave of height $a_i = 0.1$ which passes over a submerged sill of breadth D/l = 0.947 compared to the unobstructed amplitude evolution; (b) $a_i = 0.3$, D/l = 1.64; (c) $a_i = 0.4$, D/l = 5.68; (d) $a_i = 0.5$, D/l = 6.35. The vertical dashed lines represent the location of the submerged sill. ▶: amplitudes measured by the wave gauges, \triangleright : amplitudes measured by the LIF technique, $-\cdot-\cdot$, prediction by (3.1) and (3.2).

breadth of the sill is small relative to the length of the solitary wave and relatively small wave amplitude, see (2.2).

3.2. Small perturbation

Figure 3(b) shows the temporal variation of the water surface η for a wave of height $a_i = 0.3$ passing over a submerged sill of breadth D/l = 1.64. Immediately after the sill, a dispersive wavetrain begins to form off the trailing end of the transmitted solitary wave. Further on, the trailing wavetrain continues to develop with increasing wavelengths. Although not shown for brevity, the wave gauge at x = 34.8 detected a very small wave reflected from the upstream edge of the sill: the amplitude of the reflected wave is too small to quantify due to the wave gauge resolution (≈ 0.18 mm).

Figure 4(b) shows the wave amplitude evolution. The dashed lines represent the location of the submerged sill. The amplitude evolution follows the progression of the unobstructed case until it encounters the submerged sill. As the wave passes over the submerged sill, the amplitude increases (relative to the unobstructed case) in the local vicinity of the submerged sill. This localized amplification is followed by a decrease in the wave amplitude, which proceeds to then match up with the unobstructed amplitude evolution. Similar behaviour, categorized as 'small perturbation', is observed for the cases of $(a_i = 0.2, D/l = 1.34)$, $(a_i = 0.2, D/l = 2.68)$ and $(a_i = 0.1, D/l = 2.84)$ (see table 1).

In short, after passing through the sill, the solitary wave re-emerges but with a dispersive trailing wavetrain. In spite of the formation of the trailing wavetrain, it appears that the amplitude of the solitary wave is recovered to the unobstructed level by the end of the wave tank: the energy dispersion is unnoticeably small.

3.3. Large perturbation

Figure 3(c) shows the temporal variation of the water surface η for a wave of height $a_i = 0.4$ passing over the sill of breadth D/l = 5.68. The wave profile deforms as it passes over the sill. Similar to the small perturbation case, a trailing dispersive wavetrain forms at the end of the submerged sill. By the end of the wave tank, the leading wave recovers to a solitary wave with reduced amplitude and a trailing dispersive wavetrain. Although not shown for brevity, the reflected wave from the upstream edge of the sill recorded at x = 34.8 is very small (again, the amplitude cannot be resolved with the wave gauge precision ≈ 0.18 mm).

The wave amplitude evolution is shown in figure 4(c). The dashed lines represent the location of the submerged sill. The amplitude evolution follows the unobstructed case until it encounters the sill. As the wave propagates over the sill, there is a sharp increase in amplitude that continues toward the end of the sill. The amplification is followed by a sharp decrease in amplitude. While the leading wave appears to eventually take the form of a solitary wave, the amplitude remains smaller than the condition with no obstruction. The ratio of the leading wave amplitude to that of the case with no obstruction is 0.92, which corresponds to a 11.6% reduction in mechanical energy. The majority of lost energy must be transferred to the creation of the dispersive trailing wavetrain. Additionally, some of this energy is dissipated through turbulence associated with flow separation at both upstream and downstream edges of the sill. (Note that flow separation must occur at the salient edges of the sill. Energy dissipation associated with such flow separation was discussed by Chang et al. (2001).) This is in contrast to the small perturbation case where the solitary wave manages to recover to its unobstructed amplitude. Incidentally, the total mechanical energy, E, the sum of kinetic and potential energies, is computed by

$$E = \int_{-\infty}^{\infty} \int_{-h}^{\eta} \left(\frac{1}{2} \rho (u^2 + w^2) + \rho g z' \right) dz' dx, \tag{3.3}$$

assuming the waves at locations 11 and 12 (see figure 3) are expressed by (2.1). In (3.3), ρ is the fluid density, w is the vertical velocity component obtained from continuity, and we take $u = \bar{u}$, the depth-averaged horizontal velocity component. The per cent (%) loss of the total mechanical energy in comparison to the corresponding unobstructed solitary wave is listed in table 1.

The behaviour, categorized as 'large perturbation', is also observed for the cases of $(a_i = 0.4, D/l = 1.89)$, $(a_i = 0.5, D/l = 2.12)$, $(a_i = 0.3, D/l = 3.28)$, $(a_i = 0.4, D/l = 3.28)$ D/l = 3.79), $(a_i = 0.2, D/l = 4.02)$ and $(a_i = 0.3, D/l = 4.92)$. (see table 1). In short, the large perturbation is characterized by the formation of trailing dispersive wavetrain following the leading solitary wave, which experiences a reduction in amplitude. The wave amplitude does not return to the unobstructed level by the end of the wave tank.

3.4. Wave breaking

Under certain conditions, breaking of the solitary wave occurs. Footage from the LIF technique indicates the formation of a spilling-type breaker. Wave breaking can occur either as the wave passes over the sill, or shortly after the sill. In both cases, a trailing wavetrain is generated that follows the leading wave.

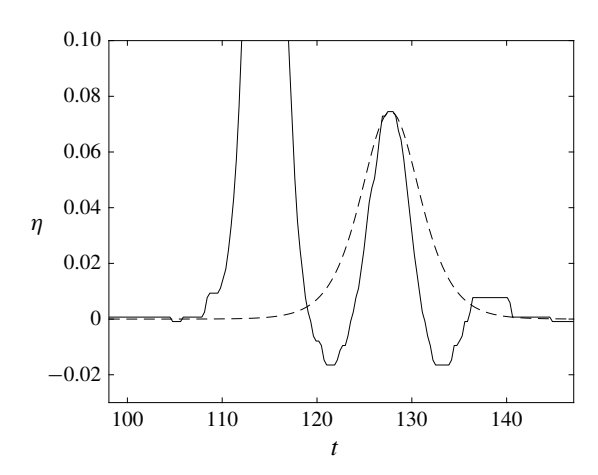


FIGURE 5. Detail of trailing wave shown in figure 3(d). The dashed line --- is solitary-wave profile by (2.1).

3.4.1. Wave breaking over sill

Figure 3(d) shows the time variation of the water surface η for the incident wave amplitude $a_i = 0.5$ which passes over a sill of breadth D/l = 6.35 (wide sill). For this large nonlinear wave, the solitary wave at the first measurement location appears to be slightly deformed in figure 3(d); however, detailed measurement with the LIF technique (not shown for brevity) indicates that the generated waveform is very close to that of a solitary wave expressed by (2.1). The slight deformation that appears in figure 3(d) must be due to the insufficient wave gauge resolution. A relatively large trailing wave forms over the sill and appears to separate from the leading transmitted wave as the wave progresses. Figure 5 shows that this trailing wave is not a solitary wave; hence it is anticipated to disperse and to become a trailing wavetrain at some distance away, though there is not enough propagation space to observe this in the present wave tank.

Figure 4(d) shows the wave amplitude evolution for the case shown in figure 3(d)compared to the unobstructed amplitude decay rate. The amplitude evolution shows the wave amplitude increases on the sill and decreases significantly after breaking. However, it is difficult to observe the detailed wave breaking process from the wave gauge measurement alone. Here we present the data acquired from the LIF technique applied in the local vicinity of the submerged sill. Figure 6(a) shows a waterfall plot for this case $(a_i = 0.5, D/l = 6.35)$. The vertical dashed lines represent the beginning and end of the submerged sill. Six time snaps of the waterfall plot are depicted in bold to represent different phases of the breaking process. Figure 6(b) shows the variation of the wave amplitude and the third moment of water-surface elevation η , which represents the horizontal asymmetry of the wave profile. The normalized horizontal asymmetry, s, is evaluated as

$$s = \int_{-\infty}^{\infty} (t - \bar{t})^3 \eta \, \mathrm{d}t / \left(\int_{-\infty}^{\infty} (t - \bar{t})^2 \eta \, \mathrm{d}t \right)^{3/2}, \tag{3.4}$$

where

$$\bar{t} = \int_{-\infty}^{\infty} t\eta \, dt / \int_{-\infty}^{\infty} \eta \, dt.$$
 (3.5)

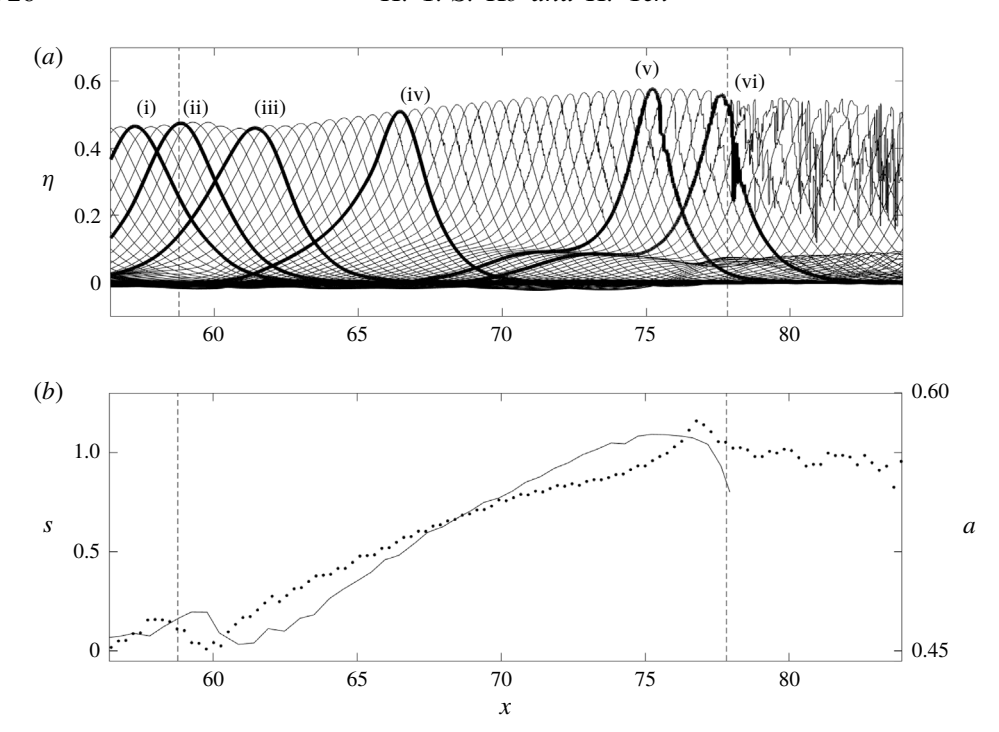


FIGURE 6. LIF measurements that show (a) a waterfall plot of the temporal water-surface profiles for a wave of amplitude $a_i = 0.5$ which passes over a submerged sill of breadth D/l = 6.35 (wide sill), and (b) variations of wave amplitude a, —, and the horizontal asymmetry, s, computed by $(3.4), \dots$ The vertical dashed lines (---) represent the beginning and end of the submerged sill. The time interval in the profiles is $\Delta t = 0.03$ s. Six distinguished transformation stages (i) through (iv) in (a) are discussed in the text.

To compute the asymmetry, the integrals in (3.4) and (3.5) were approximated by taking the limits of $\pm \infty \to \pm t$ where $\eta \ge 0.1a$. Note that a positive value of s represents the waveform being tilted forward, and a negative value represents the waveform being tilted backward.

Examination of figure 6 illuminates the following characteristics in six phases:

- (i) Incident wave upstream of the sill showing its symmetrical solitary-wave profile.
- (ii) Slight increase in wave amplitude prior to the upstream edge due to the minute wave reflection.
- (iii) Reduction in amplitude and increase in horizontal asymmetry immediately after crossing over the upstream edge.
- (iv) Gradual increase in wave amplitude and asymmetry over the sill plateau; wave leans forward. Wave profile narrows and begins to show formation of single trailing dispersive wave. Here we observe the formation of roughness on the front face of the solitary wave. This surface roughness is interpreted as the appearance of capillary waves. Such formation of capillary waves prior to the wave breaking is known to be an indication of the onset of the development of a spilling breaker (Longuet-Higgins 1994; Duncan et al. 1999; Duncan 2001).
- (v) Wave amplitude reaches its maximum amplification and begins to break. This occurs prior to the wave reaching its maximum horizontal asymmetry with a

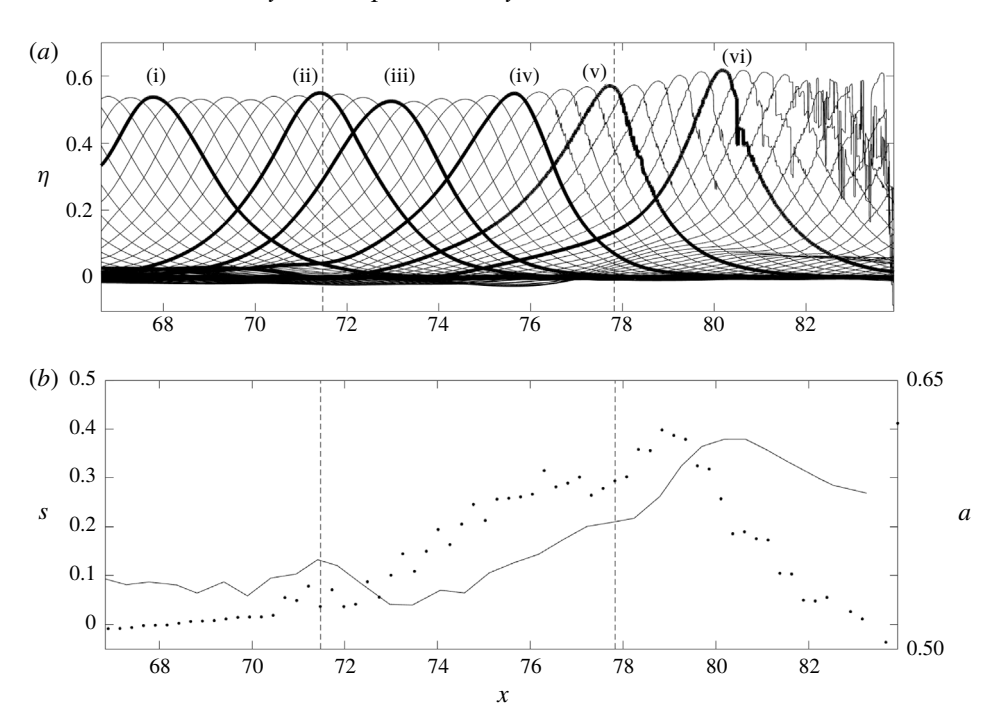


FIGURE 7. LIF measurements that show (a) a waterfall plot of the temporal water-surface profiles for a wave of height $a_i = 0.6$ which passes over a submerged sill of breadth D/l = 2.32 (narrow sill), and (b) variations of wave amplitude a, —, and the horizontal asymmetry, s, computed by $(3.4), \cdots$. The vertical dashed lines (---) represent the beginning and end of the submerged sill. The time interval in the profiles is $\Delta t = 0.03$ s. Six distinguished transformation stages (i) through (iv) in (a) are discussed in the text.

sharp increase. A small wave hump is formed on the lee side of the wave that will develop into a dispersive trailing wave.

(vi) Wave is broken and amplitude decreases. After the incipience of wave breaking, the horizontal asymmetry remains high: i.e. the waveform continues to be tilted forward with the breaking process.

3.4.2. Wave breaking downstream of sill

The case of a solitary wave with incident wave amplitude $a_i = 0.6$ passing over a submerged sill of breadth D/l = 2.32 (narrow sill) results in the occurrence of wave breaking downstream of the sill. Note that this is different than the previous case where the wave breaks on top of the sill (figure 6). Recall that the sill breadth in the previous case discussed in §3.4.1 is D/l = 6.35: substantially wider than this case. Figure 7 shows the LIF measurements performed in the local vicinity of the submerged sill. Figure 7(a) is a waterfall plot of the temporal wave profiles that shows the transformation of the wave leading to its breaking. The vertical dashed lines represent the beginning and end of the submerged sill. Six time snaps of the waterfall plot are depicted in bold to represent different phases of the breaking process, similar to the phases presented in figure 6.

Figure 7(b) shows the variation of wave amplitude and horizontal asymmetry evaluated by (3.4). Comparing the cases presented in figures 6 and 7, we notice that the wave amplitude of each case increases slightly prior to reaching the upstream edge of the sill, followed by an amplitude reduction once the wave crest climbs onto the sill. This slight amplitude increase and decrease must be related to the excess vertical component of velocity created by the upward step of the sill. The transmitted wave proceeds to shoal over the sill and increase in wave amplitude while decreasing in wavelength due to the shallower water on the plateau of the sill.

The wave breaking process is similar to that observed in figure 6(b), except that figure 7(b) shows that the breaking occurs downstream of the sill, instead of the location over the sill observed in figure 6(b). Note that the wave continues to increase in amplitude as it propagates beyond the downstream edge of the sill. This feature was observed by Cooker et al. (1990) and Grilli et al. (1994) in their numerical experiments. More importantly, the wave asymmetry rapidly increases immediately after the downstream edge of the sill. The horizontal asymmetry reaches its maximum value prior to the occurrence of the maximum amplitude. This is opposite to the previous case of breaking demonstrated in figure 6, where the maximum asymmetry happens after the maximum wave amplification associated with the breaking incipience. The horizontal asymmetry reduces to nil, quickly recovering the symmetrical form of the solitary wave. This behaviour indicates that the breaking phenomenon for this case $(a_i = 0.6, D/l = 2.32)$ lasts only for a short duration.

For the case where the wave breaks on top of the sill (figure 6), the wave amplitude increases until breaking, following typical shoaling behaviour. When D/l is small (figure 7), the wave continues to increase in amplitude beyond the downstream edge of the sill until it breaks. When the wave is large, the wave deforms and tilts forward by the presence of the sill, which triggers the wave breaking. In other words, unlike the case shown in figure 6, the disturbance of the narrow sill causes this asymmetric deformation prior to the amplitude enhancement that eventually leads to the breaking at the leeside of the sill. The submerged sill forces the solitary wave to exceed a certain amplitude threshold which creates a nonlinear instability to lead wave breaking. This instability prevents the solitary wave from recovering and continues to grow regardless of whether or not the submerged sill is still underneath the wave crest. Since less time is spent on the sill, only waves with initially larger amplitudes can cross the instability threshold. Thus, for shorter breadths of the sill, only highly nonlinear waves break. We observe this in our experiments as only a solitary wave with its initial amplitude $a_i \gtrsim 0.59$ breaks over the narrow sill (D/l = 2.32). Note that this observation is based on a series of our experiments performed with $0.5 \le a_i \le 0.6$ with the use of LIF, although clear identification of 'breaking' is subtle even with the LIF data analysis.

4. Discussion

To examine the effect of sill's breadth, we isolate a specific wave amplitude. Figure 8 shows the temporal variations of the water surface η measured at x = 74.7(above the sill: gauge location (6) as indicated in figure 1) and x = 126 (near the end of the tank: gauge location (12)), respectively, for a wave with $a_i = 0.3$ passing over each submerged sill configuration. The time axes for each of the individual time series are adjusted such that the profiles match up for more convenient comparison. Figure 8(a) shows that the wave amplification on the sill increases with sill breadth. Additionally, it appears that the wave leans forward and that trailing wave formation is more significant for wider sill breadths. Figure 8(b) shows that dispersive wave formation trailing the transmitted wave is apparent for all the cases with $a_i = 0.3$. The

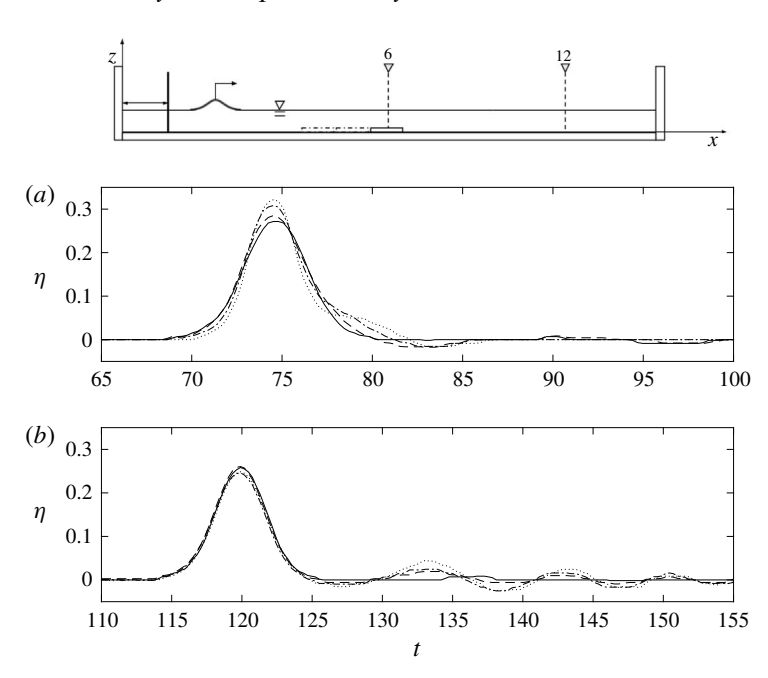


FIGURE 8. Time variation of the water-surface elevation measured at (a) x = 74.7(downstream end of sill: the gauge location 6 (see figure 1)) and (b) x = 126.0 (furthest propagation point in wave tank: the gauge location 12) for a wave with $a_i = 0.3$ passing over each submerged sill configuration: —, no sill; ---, D/l = 1.64; ----, D/l = 1.643.28; \dots , D/l = 4.93. The time axes for each profile are adjusted such that the profiles match up for more convenient comparison.

amplitude of the dispersive wavetrain increases as the length scale of the submerged sill increases. (Note that the leading crest elevations of the trailing wavetrain are 0.019, 0.025 and 0.045 for the cases of D/l = 1.64, D/l = 3.28 and D/l = 4.93, respectively, although the values are not accurate owing to the resolution of the wave gauges ≈ 0.18 mm). Figure 9 shows the comparison of amplitude evolutions between the cases with different sill breadths for a wave of $a_i = 0.3$. The amplitude on the sill increases and the downstream amplitude decreases with sill breadth: the sill breadth has a significant impact on the wave-sill response which in this case can vary from a small perturbation to a large perturbation. Figures 8 and 9 show that an increase in sill breadth can lead to larger perturbations. The maximum amplitude depends on the amount of time that the waves spend over the sill. All of the waves eventually recover to a solitary wave by the end of the wave tank with a small change in amplitude. Trailing waves are also similar but have higher amplitude for the cases with longer sill breadths.

Figure 10 graphically presents the responses observed for the 18 experimental cases shown in table 1. The wave responses appear to depend on the effect of nonlinearity a_i and the relative length scale D/l. The type of response can be ranked based on the size of the perturbation such as (from small to large): unperturbed \rightarrow small perturbation \rightarrow large perturbation \rightarrow breaking. As the perturbation increases, the solitary wave loses its ability to recover. This is first observed in the large perturbation case where the solitary-wave amplitude remains reduced (no recovery) far beyond the sill. When the perturbation becomes sufficiently large, the

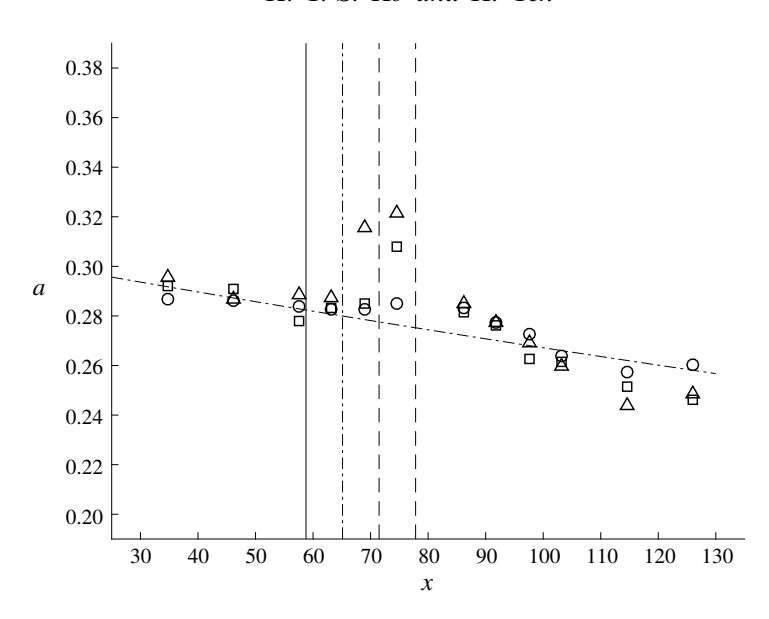


FIGURE 9. Comparison of amplitude evolution between different sill breadths for a wave with amplitude $a_0 = 0.3$: \bigcirc , D = 6.35; \square , D = 12.70; \triangle , D = 19.05; ----, prediction by (3.1) and (3.2).

perturbation continues to grow beyond the sill until the wave breaks. From figure 10, we can see that the size of perturbation increases with both parameters D/l and a_i . Note that for solitary waves, a_i and l are not independent. A larger wave amplitude, a_i , corresponds to a shorter wavelength, l. Since wavelength is proportional to $a_i^{-1/2}$ sill breadth, D/l, increases as a_i increases. Thus, the length scale of the submerged sill has a clear effect on the type of transformation that the solitary wave experiences over the sill.

Figure 10 expresses per cent (%) losses δE of mechanical energy relative to the corresponding unobstructed solitary wave. The energies are computed by (3.3) and listed in table 1. The resulting relative energy loss indicates that the longer the D/l the greater the loss. The loss sharply increases for the breaking-wave cases due to energy dissipation associated with the induced turbulence. Among the breaking-wave cases, energy dissipation turns out to be smaller when D/l is small than that for when D/lis large. For the cases presented in § 3.4, the relative energy dissipation for the case of breaking over the wide sill (D/l = 6.35) is 23.1 %, which is significantly larger than the 7.1 % dissipation for the case where breaking occurred downstream of the narrow sill (D/l = 2.32). For a short-breadth sill, while some energy dissipates by breaking, most of the energy must be recovered immediately after the wave passes over the sill. On the other hand, the wide sill sustains continual wave breaking for a long time, which allows for sufficient dissipation. As discussed in §§ 3.4.1 and 3.4.2, the variation of the horizontal asymmetry, s, differed based on the value of D/l. When D/l is small, the increase in horizontal asymmetry is temporary and the symmetrical waveform is recovered quickly after breaking. When D/l is large, the value of s persists with wave breaking after the wave passes over the sill.

For non-breaking cases, the energy reduction must result from energy dissipation through turbulence associated with flow separation caused at the salient edges of the sill, as well as energy reflection and dispersion in the form of a trailing wavetrain.

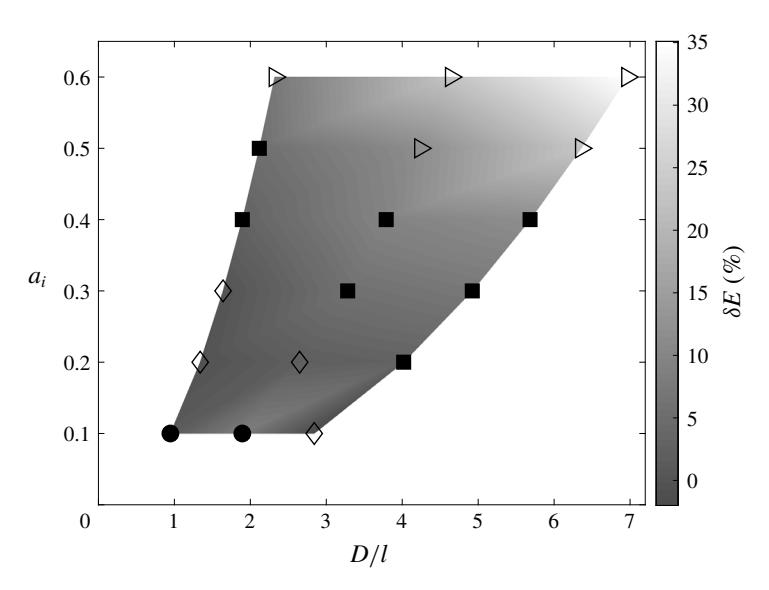


FIGURE 10. Solitary-wave responses observed for the 18 experimental cases, also listed in table 1: ●, unperturbed; ♦, small perturbation; ■, large perturbation; ▷, wave breaking. The background grey shade represents energy losses δE relative to the corresponding unobstructed solitary wave: see table 1.

The amount of energy reduction is much smaller for non-breaking waves cases than for the breaking waves cases.

5. Conclusions

Laboratory experiments are performed to study the effect of a rectangular-shaped broad sill on solitary-wave deformation and evolution during and after passing through a sill. Based on the experimental results, the following conclusions are drawn:

- (i) Four different responses of solitary waves are identified. They are classified as 'unperturbed', 'small perturbation', 'large perturbation' and 'wave breaking'. These different interactions are described in § 3. For very small perturbations (classified as 'unperturbed'), the solitary wave does not appear to be affected at all. For small perturbations, the solitary wave amplitude is locally amplified but recovers to its initial state with the formation of small dispersive trailing waves. As the perturbations get larger, the solitary-wave amplitude does not recover entirely and a noticeable trailing dispersive wavetrain is formed. At a certain size, the perturbations cause the wave to break.
- (ii) The different wave responses depend largely on the wave amplitude and sill breadth, and can be divided up into regions of the $(a_i, D/l)$ parameter space (see figure 10).
- (iii) For a single wave amplitude $a_i = 0.3$, the sill breadth has a clear effect on amplification of the wave amplitude and the type of wave response that occurs (see $\S 4$).
- (iv) Detailed wave transformation leading to wave breaking by the presence of the sill is captured with the use of the LIF technique. Considering the amplitude and horizontal asymmetry variations, the observed pre-breaking behaviours can

be explained by the effect of amplitude dispersion. The tilted sawtooth-like wave formation enhances the instability that leads to breaking. The relative timing of the maximum wave amplitude to peak horizontal asymmetry differed based on where the wave breaking occurred relative to the sill. For the case where wave breaking occurred on top of the sill, the maximum amplitude precedes the peak horizontal asymmetry, and the asymmetry persists with a prolonged wave-breaking process that results in substantial energy dissipation. When the wave breaking occurs beyond the downstream edge of the sill, however, the peak horizontal asymmetry precedes the maximum amplitude and the asymmetry subsides to nil, quickly recovering its solitary-wave form.

Acknowledgement

partially supported by the US National Science Foundation (OCE-1830024).

REFERENCES

- CARRIER, G. F., WU, T. T. & YEH, H. 2003 Tsunami run-up and draw-down on a plane beach. J. Fluid Mech. 475, 79-99.
- CHANG, K.-A., HSU, T.-J. & LIU, P. L.-F. 2001 Vortex generation and evolution in water waves propagating over a submerged rectangular obstacle: Part I. Solitary waves. Coast. Engng 44 (1), 13-36.
- CHANG, K.-A., HSU, T.-J. & LIU, P. L.-F. 2005 Vortex generation and evolution in water waves propagating over a submerged rectangular obstacle: Part II: Cnoidal waves. Coast. Engng 52 (3), 257–283.
- CHEN, Y.-S. & YEH, H. 2014 Laboratory experiments on counter-propagating collisions of solitary waves. Part 1. Wave interactions. J. Fluid Mech. 749, 577–596.
- CHRISTOU, M., SWAN, C. & GUDMESTAD, O. T. 2008 The interaction of surface water waves with submerged breakwaters. Coast. Engng 55 (12), 945–958.
- COOKER, M. J., PEREGRINE, D. H., VIDAL, C. & DOLD, J. W. 1990 The interaction between a solitary wave and a submerged semicircular cylinder. J. Fluid Mech. 215, 1-22.
- DEAN, R. G. & DALRYMPLE, R. A. 1991 Water Wave Mechanics for Engineers and Scientists, vol. 2. World Scientific Publishing Co Inc.
- DIORIO, J. D., LIU, X. & DUNCAN, J. H. 2009 An experimental investigation of incipient spilling breakers. J. Fluid Mech. 633, 271-283.
- DOLD, J. W. & PEREGRINE, D. H. 1986 An efficient boundary-integral method for steep unsteady water waves. Numer. Meth. Fluid Dyn. II 671-679.
- DUNCAN, J. H. 2001 Spilling breakers. Annu. Rev. Fluid Mech. 33 (1), 519–547.
- DUNCAN, J. H., PHILOMIN, V., BEHRES, M. & KIMMEL, J. 1994 The formation of spilling breaking water waves. Phys. Fluids 6 (8), 2558-2560.
- DUNCAN, J. H., QIAO, H., PHILOMIN, V. & WENZ, A. 1999 Gentle spilling breakers: crest profile evolution. J. Fluid Mech. 379, 191-222.
- GARDARSSON, S. M. & YEH, H. 2007 Hysteresis in shallow water sloshing. J. Engng Mech. 133 (10), 1093–1100.
- GORING, D. G. 1978, Tsunamis-the propagation of long waves onto a shelf. Rep. No. KH-R-38, California Institute of Technology.
- GRILLI, S. T., LOSADA, M. A. & MARTIN, F. 1994 Characteristics of solitary wave breaking induced by breakwaters. J. Waterways Port Coast. Ocean Engng 120 (1), 74–92.
- GRIMSHAW, R. 1971 The solitary wave in water of variable depth. Part 2. J. Fluid Mech. 46 (3),
- GRUE, J. 1992 Nonlinear water waves at a submerged obstacle or bottom topography. J. Fluid Mech. **244**, 455–476.

- HSIAO, S.-C., HSU, T.-W., LIN, T.-C. & CHANG, Y.-H. 2008 On the evolution and run-up of breaking solitary waves on a mild sloping beach. Coast. Engng 55 (12), 975–988.
- HUANG, C.-J. & DONG, C.-M. 1999 Wave deformation and vortex generation in water waves propagating over a submerged dike. Coast. Engng 37 (2), 123-148.
- HUANG, C.-J. & DONG, C.-M. 2001 On the interaction of a solitary wave and a submerged dike. Coast. Engng 43 (3-4), 265-286.
- KEULEGAN, G. H. 1948 Gradual damping of solitary waves. J. Res. Natl Bur. Stand. 40 (6), 487–498. KNOWLES, J. & YEH, H. 2018 On shoaling of solitary waves. J. Fluid Mech. 848, 1073–1097.
- KOBAYASHI, N., DESILVA, G. S. & WATSON, K. D. 1989 Wave transformation and swash oscillation on gentle and steep slopes. J. Geophys. Res. 94 (C1), 951–966.
- KOBAYASHI, N., OTTA, A. K. & ROY, I. 1987 Wave reflection and run-up on rough slopes. J. Waterways Port Coast. Ocean Engng 113 (3), 282-298.
- LI, W., YEH, H. & KODAMA, Y. 2011 On the mach reflection of a solitary wave: revisited. J. Fluid Mech. 672, 326–357.
- LI, Y. & RAICHLEN, F. 2003 Energy balance model for breaking solitary wave runup. J. Waterways Port Coast. Ocean Engng 129 (2), 47-59.
- LIN, C., CHANG, S.-C., HO, T.-C. & CHANG, K.-A. 2006 Laboratory observation of solitary wave propagating over a submerged rectangular dike. J. Engng Mech. 132 (5), 545-554.
- LIN, M.-Y. & HUANG, L.-H. 2010 Vortex shedding from a submerged rectangular obstacle attacked by a solitary wave. *J. Fluid Mech.* **651**, 503–518.
- LIN, P. 2004 A numerical study of solitary wave interaction with rectangular obstacles. Coast. Engng **51** (1), 35–51.
- LIN, P., CHANG, K.-A. & LIU, P. L.-F. 1999 Runup and rundown of solitary waves on sloping beaches. J. Waterways Port Coast. Ocean Engng 125 (5), 247-255.
- LIN, P. & LIU, H.-W. 2005 Analytical study of linear long-wave reflection by a two-dimensional obstacle of general trapezoidal shape. J. Engng Mech. 131 (8), 822-830.
- LIU, P. L.-F. & CHENG, Y. 2001 A numerical study of the evolution of a solitary wave over a shelf. Phys. Fluids 13 (6), 1660-1667.
- LONGUET-HIGGINS, M. S. 1994 Shear instability in spilling breakers. Proc. R. Soc. Lond. A 446 (1927), 399-409.
- LOSADA, I. J., SILVA, R. & LOSADA, M. A. 1996 Interaction of non-breaking directional random waves with submerged breakwaters. Coast. Engng 28 (1-4), 249-266.
- LOSADA, M. A., VIDAL, C. & MEDINA, R. 1989 Experimental study of the evolution of a solitary wave at an abrupt junction. J. Geophys. Res. 94 (C10), 14557-14566.
- MASSEL, S. R. 1983 Harmonic generation by waves propagating over a submerged step. Coast. Engng 7 (4), 357–380.
- MEI, C. C. & BLACK, J. L. 1969 Scattering of surface waves by rectangular obstacles in waters of finite depth. J. Fluid Mech. 38 (3), 499-511.
- MEI, C. C. & LIU, L. F. 1973 The damping of surface gravity waves in a bounded liquid. J. Fluid Mech. 59 (2), 239-256.
- MILES, J. W. 1967 Surface-wave damping in closed basins. Proc. R. Soc. Lond. A 297 (1451), 459-475.
- PEDERSEN, G. & GJEVIK, B. 1983 Run-up of solitary waves. J. Fluid Mech. 135, 283–299.
- RAMSDEN, J. D. & RAICHLEN, F. 1990 Forces on vertical wall caused by incident bores. J. Waterway, Port, Coastal, and Ocean Engineering 116, 592-613.
- V., BELZONS, M. & GUAZZELLI, E. 1992 Propagation of surface gravity waves over a rectangular submerged bar. J. Fluid Mech. 235, 453-479.
- SEABRA-SANTOS, F. J., RENOUARD, D. P. & TEMPERVILLE, A. M. 1987 Numerical and experimental study of the transformation of a solitary wave over a shelf or isolated obstacle. J. Fluid Mech. 176, 117–134.
- SYNOLAKIS, C. E. 1987 The runup of solitary waves. J. Fluid Mech. 185, 523-545.
- TANAKA, M. 1993 Mach reflection of a large-amplitude solitary wave. J. Fluid Mech. 248, 637-661.
- TANG, C.-J. & CHANG, J.-H. 1998 Flow separation during solitary wave passing over submerged obstacle. J. Hydraulic Engng 124 (7), 742–749.

- TING, F. C. K. & KIM, Y.-K. 1994 Vortex generation in water waves propagating over a submerged obstacle. Coast. Engng 24 (1-2), 23-49.
- YASUDA, T., MUTSUDA, H. & MIZUTANI, N. 1997 Kinematics of overturning solitary waves and their relations to breaker types. Coast. Engng 29 (3-4), 317-346.
- YEH, H. & GHAZALI, A. 1987 A bore on a uniformly sloping beach. In Proc. 20th Intl Conf. on Coastal Engng, pp. 877-888. ASCE.
- YEH, H., KO, H., KNOWLES, J. & HARRY, S. 2019 Solitary waves perturbed by a broad sill. Part 2. Propagation along the sill. J. Fluid Mech. (in press).
- YOUNG, D. M. & TESTIK, F. Y. 2011 Wave reflection by submerged vertical and semicircular breakwaters. Ocean Engng 38 (10), 1269–1276.
- ZHUANG, F. & LEE, J.-J. 1997 A viscous rotational model for wave overtopping over marine structure. In Proc. 25th Intl Conf. Coastal Engng, pp. 2178-2191. ASCE.